minerals

MDPI

Article

The Role of Organic Matter in the Formation of High-Grade Al Deposits of the Dopolan Karst Type Bauxite, Iran: Mineralogy, Geochemistry, and Sulfur Isotope Data

Somayeh Salamab Ellahi, Batoul Taghipour * and Mostafa Nejadhadad

Department of Earth Sciences, Shiraz University, Shiraz 71454, Iran; somayesalamat@yahoo.com (S.S.E.); mostafanejadhadad@yahoo.com (M.N.)

* Correspondence: taghipour@shirazu.ac.ir; Tel.: +98-713-613-7457

Academic Editor: Pablo Cubillas

Received: 23 March 2017; Accepted: 31 May 2017; Published: 12 June 2017

Abstract: Mineralogical and geochemical analyses of the Dopolan karstic bauxite ore were performed to identify the characteristics of four bauxite horizons, which comprise from top to bottom, bauxitic kaolinite, diaspore-rich bauxite, clay-rich bauxite, and pyrite-rich bauxite. Diaspore, kaolinite, and pyrite are the main minerals; böhmite, muscovite, rutile, and anatase are the accessory minerals. The main minerals of the Dopolan bauxite deposit indicate slightly acidic to alkaline reducing conditions during bauxitization. Immobile elements (Nb, Ta, Zr, Hf, and rare earth elements) are enriched in the diaspore-rich horizon, which also has the highest alumina content, whereas redox sensitive elements (e.g., Cr, Cu, Ni, Pb, Zn, Ag, U, and V) are enriched in the lowest horizon of pyrite-rich bauxite. The presence of a high content of organic matter was identified in different horizons of bauxitic ore from wet chemistry. The presence of organic matter favored Fe bioleaching, which resulted in Al enrichment and the formation of diaspore-rich bauxite. The leached Fe^{2+} reacted with the hydrogen sulfur that was produced due to bacterial metabolism, resulting in the formation of the pyrite-rich horizon towards the bottom of the Dopolan bauxite horizons. Biogeochemical activity in the Dopolan bauxitic ore was deduced from the reducing environment of bauxitization, and the deposition of framboidal and cubic or cubic/octahedral pyrite crystals, with large negative values of $\delta^{34}S$ of pyrite ($-10‰$ to $-34‰$) and preserved fossil cells of microorganisms.

Keywords: organic matter; pyrite; Al enrichment; sulfur isotope; Dopolan bauxite

1. Introduction

Previous studies have demonstrated that differences in the mineralogical compositions of bauxite horizons could be related to different Eh and pH of the depositional environment as a result of organic matter variations in the original host rocks [1–6]. In the presence of a high content of organic matter, microorganisms, such as bacteria and fungi, convert metal compounds into their water-soluble forms. These water-soluble metals are biocatalytic productions of this leaching process [7]. Microorganisms are able to mobilize metals by (1) the formation of organic and inorganic acids, (2) oxidation and reduction reactions, and (3) the excretion of complexing agents [8–12]. Bacterial activity has an important role in the leaching of iron to alter a high-iron, low-grade red bauxite ore to a high-grade, gray alumina ore with low Fe content [2,3,13].

The bauxite deposits of the Zagros orogenic belts in southwestern Iran were deposited during two periods: (1) in karst cavities at the boundary between the Sarvak and Ilam Formations (Cretaceous bauxite deposits), such as the Mandan, Dehnow, and Sarfaryab deposits, and (2) deposited at the boundary between the Neyriz and Khaneh-Kat Formations (Triassic bauxite deposits), such as the

Dopolan deposit. Most of Iranian karst bauxites in the Zagros orogenic belts are low-grade, böhmitic, diasporic bauxites [14–17]. They contain 20–45 wt % Al_2O_3, 3–38 wt % Fe_2O_3, and in most cases appear red in outcrops. Contrastingly, the Dopolan bauxite has exceptionally high Al_2O_3 (62–78 wt %, average 65 wt %), low total Fe (0.56–32 wt %, average 5 wt %), and is almost gray in the field [18]. The Dopolan bauxite deposit has been in production for more than 40 years. Mineralization includes three separated pocket and tabular orebodies (Shahid Nilchian, Dorag, and C mine). The ore reserves total 8 to 15 million metric tonnes of 47 wt % Al_2O_3 [19].

A previous study of the Dopolan bauxite described mineralogical and geochemical characteristics of the bauxitic horizons [18]. Salamab [18] suggests that the bauxite formed as a continental deposit filling karstic cavities at the boundary of the Khaneh-Kat and Neyriz formations. The present study is focused on the organic matter rich bauxite horizons, which are characterized by an association with the abundance of pyrite. We investigated the role of organic matter and microorganisms in the mobility of trace elements, mobilization and deposition of iron, and Al enrichment in the bauxite profile. To attain these goals, the ore composition (major, trace, and rare earth elements), the organic matter content, and the sulfur isotopic values of pyrite of a series of bauxite horizons were analyzed using optical microscopy, scanning electron microscopy (SEM), X-ray diffractometry (XRD), and inductively coupled plasma mass spectrometry (ICP-MS).

2. Geology

The Dopolan bauxite deposit is located 110 km northwest of Share-Kord city, southwestern Iran (Figure 1a) [18]. The deposit is situated in the high Zagros Mountains and developed in the Triassic carbonates of the Khaneh-Kat Formation in the contact zone with the Jurassic carbonates of the Neyriz Formation. The Zagros orogenic belt extends for approximately 1500 km from Kermanshah in the northwest of Iran to Bandar Abbas in the south of the country. The Zagros zone is located in the boundary between the Arabian and Eurasian lithospheric plates. It was formed during the Cenozoic orogenic movements as a result of collision between the Arabian and Eurasian plates [20,21]. This collision created numerous folds and thrusts that now appear as large linear anticlines. Outcrops of the bauxitic horizons occur in a large structure called the Sabzkuh–Kelar anticlinorium, which is bounded by two thrust faults. The Sabzkuh anticline is 65 km long. In the studied area, the Zagros stratigraphy consists of Cambrian to Quaternary sequences. The youngest strata are located on limbs and the oldest rocks are in the core of the anticlinorium (Figure 1b). The Dalan Formation is the oldest exposed rock unit in the core of the Sabzkuh anticline. The Dopolan bauxite deposit is hosted within Triassic carbonate rocks of the Khaneh-Kat Formation. The Khaneh-Kat Formation includes dolostones, dolomitic limestones, marly limestones with interbedded marl, and argillaceous limestones overlying Permian pink dolostones of the Dalan Formation. The Dopolan bauxite deposit is stratabound and crops out in an erosional window. The boundary between the Khaneh-Kat Formation and the overlying Jurassic limestone and shaly limestone of the Neyriz Formation is an erosional unconformity that contains the Dopolan bauxite horizon. On its turn, the Neyriz formation is covered by a sequence comprising, from older to younger: the Surmeh, the Sarvak, and the Gurpi Formations [19]. Karstified features within the Khaneh-Kat Formation are infilled by bauxite. The layers of bauxite vary from 1 to 8 m in thickness and can be more than 1000 m in length.

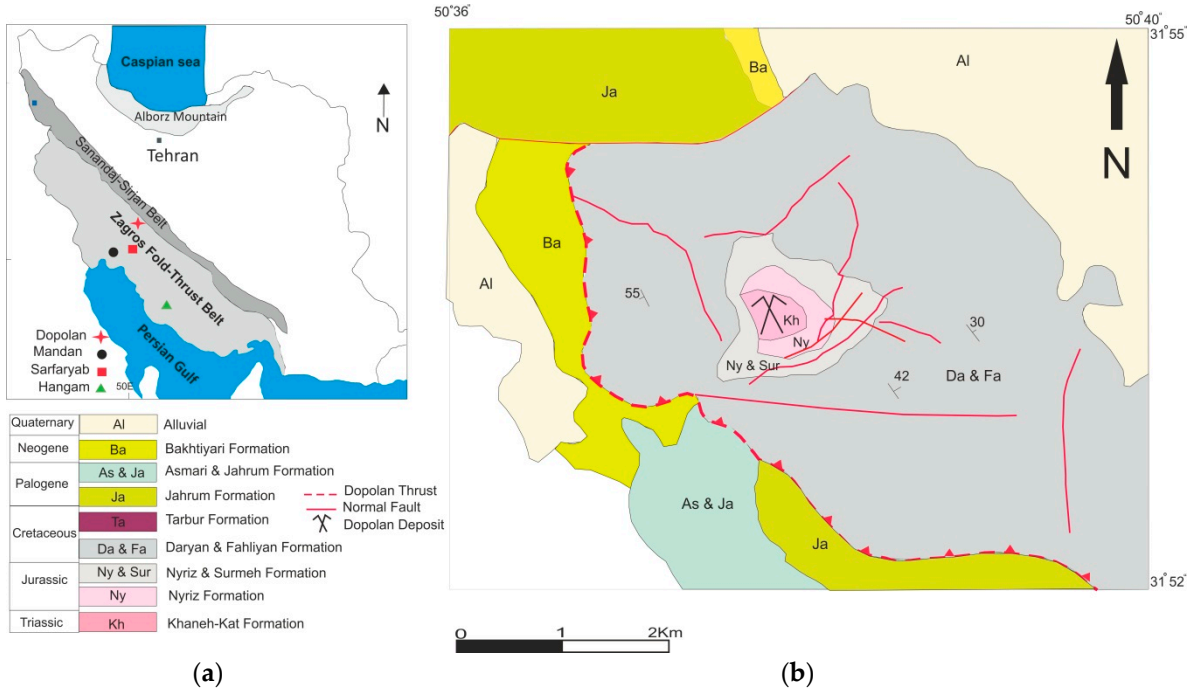

Figure 1. (**a**) Location of the Dopolan karstic bauxite in the Zagros fold belt. (**b**) Geological map of the Dopolan bauxite deposit (modified after [18]).

3. Methodology

The exposures of the Dopolan bauxite were divided into four different horizons on the basis of their macromorphological facies and their relation to the foot wall and hanging wall. A total of 28 samples, each weighing 3 kg, of different layers were selected during the fieldwork. Samples were obtained from the topmost part of the Khaneh-Kat Formation, the bauxite profiles, and the lowest part of the Neyriz Formation carbonates in three different cross-sections. Thin and polished sections were prepared for different mineralogical examinations including optical microscopy (both transmitted and reflected), SEM. SEM-Energy dispersive spectrometer (EDS) analysis was performed at the Razi Metallurgical Research Center (Iran), using a Tescan VEGAII XMU-EDS. Minerals were identified using XRD at the Kansaran Binallod, Pardis Science and Technology Park, Tehran, using a Philips X-pert PW diffractometer. The concentrations of major, trace, and rare earth elements (REE) were determined using inductively cople plasma-mass spectroscopy (ICP-MS) by ACME Analytical Lab Ltd., Vancouver, BC, Canada.

Total organic carbon (TOC) of selected samples was determined following the method of Walkey and Black [22]. In this method, organic carbon present in organic matter (OM) is oxidized by chromic acid in the presence of concentrated sulfuric acid.

The analysis of sulfur isotopes was performed on three handpicked pyrite samples and three whole-rock samples from both pyrite-rich and bauxitic kaolinite horizon samples at the University of California, Davis (UC Davis), stable isotope analysis facility (Davis, CA, USA). The δ34S was analyzed by an elemental vario isotope cube interfaced to a Ser Con 20–22 IRMS packed with tungsten oxide. The sample gases were reduced with elemental copper at 880 °C. Sample SO2 was passed directly to the isotope ratio mass Spectrometer (IRMS) for measurement. Calibration data were from standards IAEA S.1, S.2, S.3, IAEA-SO-5, IAEA-SO-6, and HHS. The results are given in per mil (‰) relative to Vienna Canon diablo Troilite (VCDT).

4. Mineralogical Characteristics

The Dopolan karst bauxite ore [18] mainly consists of diaspore, kaolinite, nacrite, and pyrite (Table 1). Böhmite, anatase, rutile, quartz, and muscovite are present as minor minerals. On the basis of the main mineral contents, the bauxite profile can be divided into four bauxite horizons: bauxitic kaolinite, diaspore-rich bauxite, clay-rich bauxite, and pyrite-rich bauxite (Figure 2).

Table 1. XRD results of the Dopolan deposit [18].

Sample No.	Bauxite Layers	Major Phases	Minor Phases
Do-org	bauxitic kaolinite	nacrite, kaolinite, pyrite	anatase, rutile
Do-oo	diaspore-rich	diaspore, nacrite	anatase, muscovite, rutile
Do-pi	diaspore-rich	diaspore	anatase, nacrite, muscovite, rutile
Do-cl	clay bauxite	kaolinite, diaspore	böhmite
Do-ir	pyrite-rich	kaolinite, pyrite, nacrite	anatase, böhmite, muscovite, rutile
Kha	Khaneh-kat dolomite	calcite, dolomite, montmorillonite	-

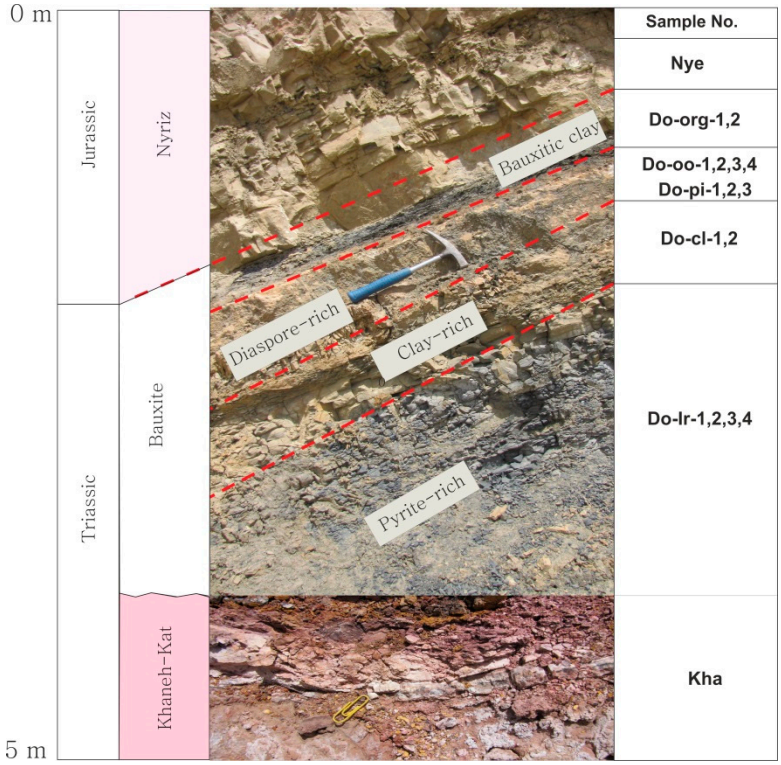

Figure 2. Schematic stratigraphic column of the Dopolan bauxite deposit.

Above the karstified dolomites of the footwall, within the pyrite-rich horizon, the main ore minerals are kaolinite, nacrite, and pyrite; whereas böhmite, muscovite, anatase, and rutile are minor minerals. Optical microscopy, XRD and SEM studies of the pyrite-rich horizon revealed abundant pyrite (20% in modal proportion to more than 35%). The pyrite-rich horizon is ~1.5 m thick. Pyrite grains are mainly framboidal and cubic in shape; some cubic-octahedral crystals are also present (Figure 3). Above the pyrite-rich horizon, in the clay-rich bauxite, the amount of pyrite decreases to less than 5% in modal proportion. The main minerals in this horizon include kaolinite and diaspore whereas böhmite is minor. The clay-rich bauxite, ~5 m thick, is gray to light gray in color and has a fine-grained oolitic texture. Up to the top of the bauxite sequence, the amount of kaolinite decreases and diaspore increases to a maximum of 80% modal. In the diaspore-rich bauxite, minor minerals include nacrite, muscovite, rutile, and anatase. The diaspore-rich bauxite is the main ore zone and is mined. The layer contains an average of 70% Al_2O_3, 3% Fe_2O_3, and 2% TiO_2 [18]. This horizon is

distinguished by its pisolitic and oolitic textures. At the top of the bauxite profile, there is a layer of black bauxitic kaolinite that is enriched in organic matter and is 0.35–1.5 m thick, indicating a large supply of organic matter in the depositional environment of this layer. In this horizon, kaolinite, nacrite, and pyrite are the main minerals whereas böhmite, diaspore, rutile, and anatase are the minor minerals. The morphology of pyrite in the bauxitic kaolinite horizon is the same as in the pyrite-rich bauxite horizon (Figure 3).

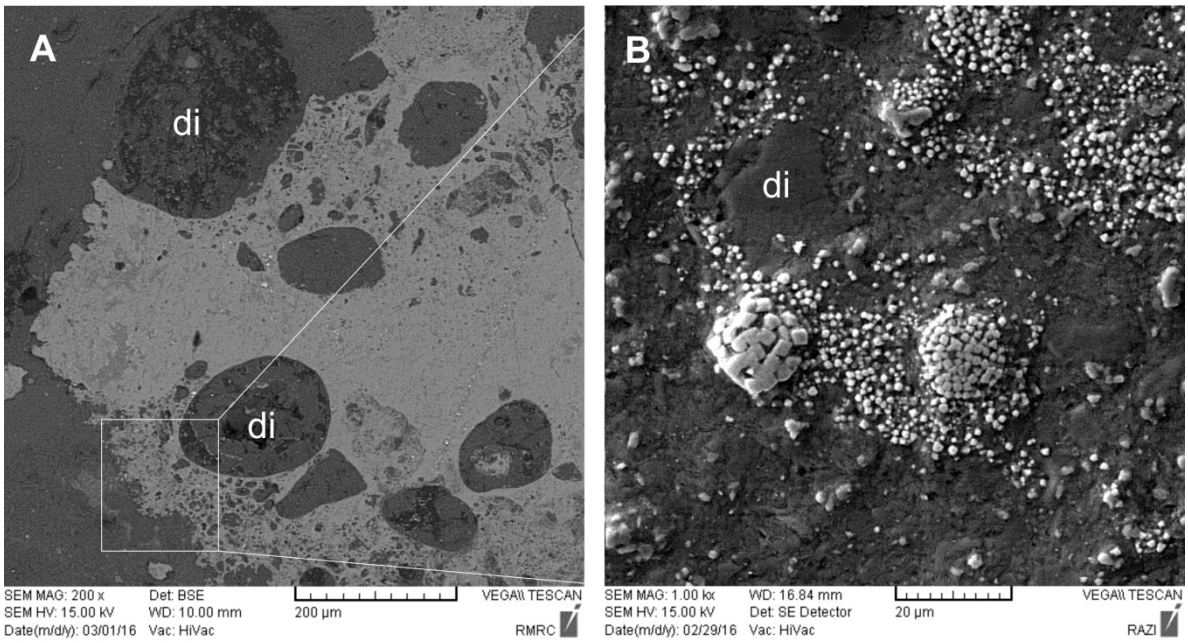

Figure 3. (**A**) Back scatters images (BSE) showing pyrite with inclusions of diasporic pisoliths (di). (**B**) Enlargement of panel A. Different morphological forms of pyrite, spherules of framboidal pyrite, and cubic pyrite. di: diaspore.

5. Geochemical Features

5.1. Distribution of Elements

The geochemical data (Table 2) confirm the mineralogical results. The aluminum, titanium, potassium, and magnesium contents decrease from the top to bottom of the bauxite profiles, i.e., from the diaspore-rich to the pyrite-rich horizon (Figure 4). In contrast, the silica and iron content increases from the diaspore-rich to the pyrite-rich horizon (Figure 4). REE and immobile elements such as the HFSE (Th, Ta, Nb, Zr, and Hf) are enriched in the diaspore-rich bauxite and decrease to the bottom of the bauxite profile (Figure 4), whereas more mobile elements of the weathering profile such as redox-sensitive elements (Zn, Cu, Ni, Co, Ag, As, U, and V) increase from top to bottom (Figure 4). The total content of mobile elements is more than twice that in the pyrite-rich bauxite compared to other horizons.

Table 2. Chemical composition of the Dopolan bauxite deposit. Measurements for major oxides and sulfur contents are in wt %; trace elements and rare earth elements (REE) are in ppm.

Horizon	**Pyrite-Rich Horizon**				**Clay-Rich Bauxite**		**Diaspore-Rich Bauxite**							**Black Bauxitic Kaolinite**	
Samples	**Do-IR-1**	**Do-IR-2**	**Do-IR-3**	**Do-IR-4**	**Do-cl-1**	**Do-cl-2**	**Do-oo-1**	**Do-oo-2**	**Do-oo-3**	**Do-oo-4**	**Do-pi-1**	**Do-pi-2**	**Do-pi-3**	**Do-org-1**	**Do-org-2**
SiO_2	7.21	16.14	14.62	11.25	35.28	31.87	7.44	5.68	5.63	3.20	4.67	5.45	3.11	34.84	35.44
Al_2O_3	42.02	31.34	37.58	47.1	47.39	50.69	68.11	67.78	68.23	72.89	74.98	73.25	75.09	31.1	26.55
Fe_2O_3	19.68	21.08	16.42	11.18	25.9	1.02	3.53	2.47	4.55	0.92	2.26	2.33	1.36	5.52	7.45
CaO	0.06	0.10	0.04	0.13	0.06	0.05	0.07	0.11	0.04	0.03	0.04	0.08	0.07	0.90	0.13
K_2O	0.51	1.16	0.61	0.85	0.80	0.36	0.30	0.65	0.80	1.21	0.25	1.64	0.29	4.06	3.83
MnO	0.01	0.02	0.01	0.00	0.00	0.00	0.00	0.00	0.00	0.00	0.00	0.00	0.02	0.03	0.00
Na_2O	0.01	0.01	0.01	0.06	0.01	0.01	0.01	0.02	0.01	0.07	0.01	0.04	0.06	0.05	0.12
P_2O_5	0.10	0.09	0.08	0.07	0.06	0.07	0.10	0.07	0.09	0.08	0.13	0.12	0.15	0.06	0.05
MgO	0.28	0.58	0.36	0.42	0.10	0.28	0.05	0.41	0.10	0.24	0.02	0.03	0.34	0.32	0.91
TiO_2	1.47	1.07	1.75	1.50	1.92	2.38	2.15	2.35	2.35	2.65	2.83	2.34	2.77	0.95	0.94
LOI	26.3	25.9	28.13	26.32	11.27	12.62	17.35	20.36	16.89	17.82	15.42	15.67	16.56	22.67	23.24
TOC	0.42	0.37	-	-	0.18	0.2	-	0.18	-	-	0.016	0.21	-	1.00	1.14
Sum	97.64	97.48	99.62	98.88	99.47	99.35	99.12	99.89	98.69	99.11	100.62	100.96	99.82	100.50	98.66
Bi	0.89	0.75	0.9	0.75	0.82	0.7	1.4	0.55	1.82	0.69	1.01	0.53	0.43	0.89	0.53
As	29	48	51	49	7.5	6	1	4.6	27.3	30	5.2	5.9	4.8	1	1
Cd	1.4	2.21	2.37	2.25	0.59	0.33	0.89	0.64	1.24	1.75	0.27	0.05	0.66	0.3	0.13
Ni	340	394	345	382	296	290	236	150	111	273	220	258	170	407	270
Co	203	179	155	197	5.2	8.3	6.4	5.7	43.1	172	143	4.6	2.7	17.9	11
Cr	429	286	577	381	359	255	486	442	389	329	132	139	303	747	1088
Cs	0.18	0.26	0.15	0.36	0.11	0.28	0.05	0.13	0.22	8.3	0.15	0.33	0.03	3.39	3.21
Cu	403	184	389	144	92	63	155	102	228	143	151	70.7	9	65.2	50.2
Pb	212	189	180	130	43	28	30	101	77	25.5	56	44	5	44	35
Hf	6.63	6.54	13.6	9.66	8.89	14.82	12.2	9.93	18.9	17.72	16.87	15.46	17.78	5.29	6.21
Ag	4.02	3.41	8.59	5.50	2.1	2.7	3.1	2.37	2.95	3.11	1.48	0.96	0.33	1.63	0.94
La	8.7	17	9.9	18.5	1	3.5	9.9	1.8	23.8	24	8.9	0.3	1.2	44.2	62.12
Ce	28.9	47.9	38.6	54	2.01	0.88	10.1	4.47	56	198	12.8	0.6	30.04	87.9	98
Pr	3.23	5.64	4.35	4.2	0.32	0.2	1.94	0.71	4.62	23.97	2.09	0.08	0.4	10.3	16.69
Nd	14.1	25	19.9	14.71	1.09	12.7	5.48	2.76	14	94.0	6.69	0.28	0.25	38.3	10.56
Sm	2.86	7.29	3.96	9.04	0.36	0.1	1.06	0.76	2.84	7.76	1.13	0.09	0.03	6.73	2.48
Eu	0.57	2.18	0.95	1.53	0.11	1.98	0.28	0.2	0.52	1.4	0.21	0.05	1.44	1.35	3.51
Gd	4.25	18.3	5.83	7.32	0.7	0.38	1.62	0.99	3.58	5.66	1.43	0.16	6.7	8.87	16.25
Dy	4.59	28.4	5.79	13.95	0.86	10.95	1.47	1.43	3.4	8.36	1.68	0.23	1.85	6.02	8.04
Ho	0.98	5.73	1.16	3.21	0.2	2.24	0.29	0.28	0.73	1.81	0.32	0.05	0.2	1.13	2.64
Er	2.86	14.9	3.75	9.9	0.63	0.74	0.79	0.87	2.27	5.48	0.99	0.2	0.8	3.38	7.34

Table 2. *Cont.*

Horizon	Pyrite-Rich Horizon				Clay-Rich Bauxite		Diaspore-Rich Bauxite							Black Bauxitic Kaolinite	
Samples	**Do-IR-1**	**Do-IR-2**	**Do-IR-3**	**Do-IR-4**	**Do-cl-1**	**Do-cl-2**	**Do-oo-1**	**Do-oo-2**	**Do-oo-3**	**Do-oo-4**	**Do-pi-1**	**Do-pi-2**	**Do-pi-3**	**Do-org-1**	**Do-org-2**
Tm	0.47	2.02	0.63	1.64	0.12	1.1	0.15	0.15	0.43	0.92	0.15	0.05	0.1	0.48	1.2
Yb	2.8	10.4	4	11.1	0.7	7.4	1	1	2.6	6.34	0.8	0.3	0.5	3	7.41
Lu	0.41	1.5	0.62	1.71	0.12	1.15	0.14	0.14	0.41	0.89	0.12	0.03	0.78	0.47	0.9
Th	24.5	25.7	34.3	36.16	21.54	49.64	44.52	28.41	46.35	51.92	38.57	38.75	54.66	10.6	17.34
Zn	96	101	197	122	144	123	145	97.2	117	120	69.5	51.5	5	48.2	21
Zr	246	250	340	364	271	583	419	308	557	535.8	467.2	437.8	478.4	206	132
Mo	4.09	8.44	3.93	6.74	25.9	20.5	15.4	21	32.3	28	3.83	13.9	7	1.35	1.4
Nb	43.1	35.3	46.2	38.34	45.6	54.43	52.6	54.7	77.7	67.9	41.4	28.4	62.4	38.2	33.8
S	>5	>5	>5	>5	1	2.1	1.4	1.5	2.5	1.75	1.2	1.4	1.2	2.2	1.7
Sb	10.6	4.44	11.7	9.65	3.89	2.52	2.74	2.34	6.53	4.33	2.84	2.51	1.99	0.36	0.23
Ta	4.58	3.87	6.21	2.72	4.4	4.97	5.35	5.19	7.2	8.1	5.6	3.1	6.4	3.6	2.9
Tl	0.19	1.12	0.2	0.56	0.18	0.1	0.12	0.14	0.37	0.25	0.09	0.21	0.38	0.18	0.22
U	67.4	70.4	111	35.05	6.8	27.12	9.2	10.2	23.4	17.4	11.1	2.3	11.6	2.6	9.4
V	1250	759	1441	472	272	310	186	330	365	485	277	304	442	107	163
Y	17.1	147	17.8	55	3.2	4.6	6	4.6	13.9	41.06	5.5	1.2	56.34	29.9	55.4

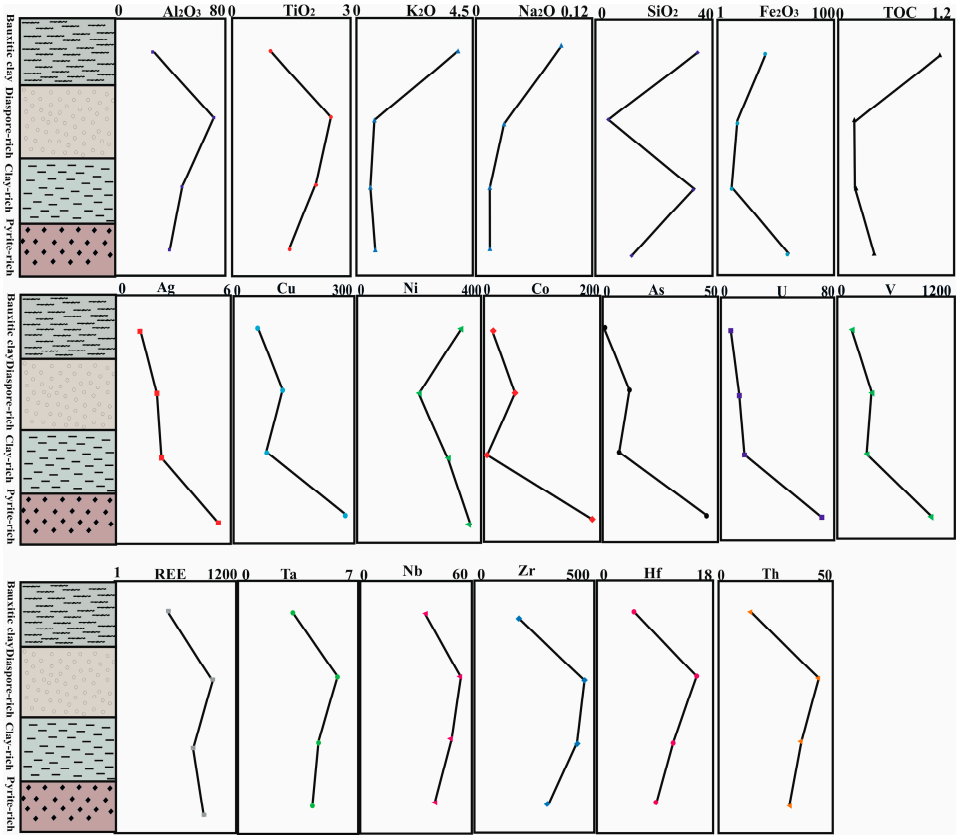

Figure 4. Variations in major oxides (in wt %), ∑REE, and selected trace elements (in ppm) in the Dopolan bauxite sequence in response to Total organic content (TOC). Points refer to the average content of the selected samples.

5.2. Organic Matter of Bauxite Horizons

The TOC content of different bauxite horizons, foot, and hanging walls of the Dopolan bauxite was calculated (Table 2) to investigate the relationship between elemental mobility and TOC. The TOC content of the Dopolan bauxite deposits varies from 0.18% in the diaspore-rich bauxite to 1% in the bauxitic kaolinite. Both the lowest and the uppermost parts of the bauxitic profile, which have higher TOC contents, have higher contents of pyrite. The alumina content of bauxite samples displays a negative correlation with TOC (Figure 5). The REE behavior in bauxite horizons is the inverse of those of Fe and TOC (Figure 4).

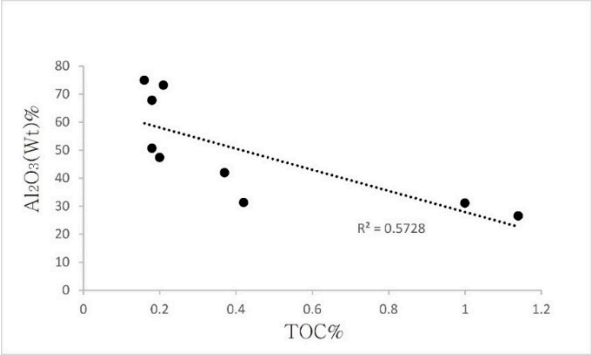

Figure 5. Al_2O_3 and TOC values of the Dopolan samples, displaying a negative correlation coefficient.

5.3. Sulfur Isotopes

The $\delta^{34}S$ values of handpicked pyrites from the pyrite-rich bauxite horizon and whole-rock from the bauxitic kaolinite and pyrite-rich bauxite samples display a wide negative range, from −10.12‰ to −34.58‰ (Table 3; Figure 6). However, the $\delta^{34}S$ values of the bauxitic kaolinite vary from −26.77‰ to −33.58‰, exhibiting a narrower range than that of the pyrite-rich bauxite samples (−10.12‰ to −34.59‰).

Table 3. Sulfur isotope compositions of pyrite and whole-rock samples from the Dopolan deposit.

Sample No.	Horizon	Description	$\delta^{34}S$
S-1	pyrite-rich	whole rock	−34.59
S-2	pyrite-rich	separated pyrite	−34.47
S-3	pyrite-rich	separated pyrite	−10.12
S-4	bauxitic kaolinite	separated pyrite	−26.77
S-5	bauxitic kaolinite	whole rock	−33.58
S-6	bauxitic kaolinite	whole rock	−28.63

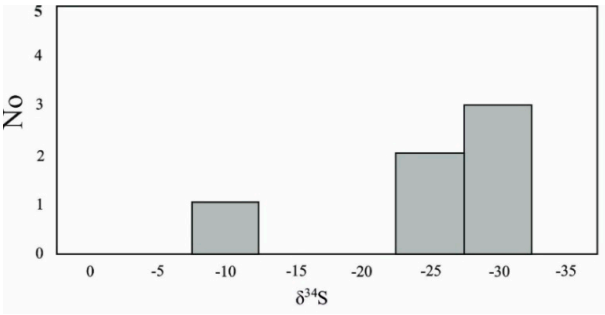

Figure 6. Frequency histogram of the $\delta^{34}S$ values of the Dopolan bauxite deposit.

6. Discussion

6.1. Formation of the Pyrite-Rich Horizon

Significant amounts of pyrite were deposited in the lowest part of the bauxite sequence of the Dopolan deposit, forming an unusual pyrite-rich horizon. The presence of Fe-oxy-hydroxide minerals in bauxitic horizons is commonly reported, but pyrite-rich bauxites are uncommon and have been described from only some areas, such as the Taurides region in Turkey [1]; the Minjera deposit, Croatia; and the gray part of the Parnassos–Ghiona bauxite deposit in Greece [3]. The TOC values of the Dopolan bauxite ore vary from 0.18% in the diaspore-rich bauxite, 0.2% in the clay-rich bauxite, 0.4% in the pyrite rich bauxite, and up to 1% in the upper bauxitic kaolinite horizon. These data indicate that the TOC content of the Dopolan bauxite is higher than that of most bauxite deposits of the world [3,4]. The high content of preserved organic matter in the gray bauxite of the Dopolan resulted in reducing conditions caused by decomposition of the organic matter. In these conditions, the sparingly soluble Fe^{3+} was reduced to more soluble Fe^{2+} [23], which is leached out from the upper part of the sequence. Microorganisms could accelerate this reaction by their enzymes or metabolism. In water-saturated soils, microbial reduction of Fe oxides in the presence of organic matter facilitates mobility and removal of iron from the soil profile [24,25]:

$$4FeOOH + CH_2O + 8H^+ = 4Fe^{2+} + CO_2 + 7H_2O.$$

Hydrogen sulfide is produced from the reduction of sulfate by a variety of bacterial species, e.g., *Desulfovibrio desulfuricans*, when organic matter as an energy source is present as a reducing agent [3,26]. The following reaction has been proposed [27–30]:

$$2\,CH_2O + SO_4^{2+} \rightarrow H_2S + 2\,HCO^{3-}$$

Bacteria fossils and associated microorganisms with the pyrite are the best evidence for the aforementioned conditions (Figure 7). The morphology of pyrite is essentially related to the degree of Fe and S saturation of pore water [31–33]. If the interstitial water is supersaturated with respect to FeS, monosulfides are deposited. When these monosulfides change to pyrite, the pyrite will have a spherulitic morphology and form clusters of well-formed grains and euhedral crystals (Figure 3). If pyrite is directly deposited from solution, the most common morphology is cubic to cubic-octahedral [34]. Therefore, the cubic-octahedral morphology of the Dopolan pyrite is due to the saturation of pore water with respect to iron and sulfur.

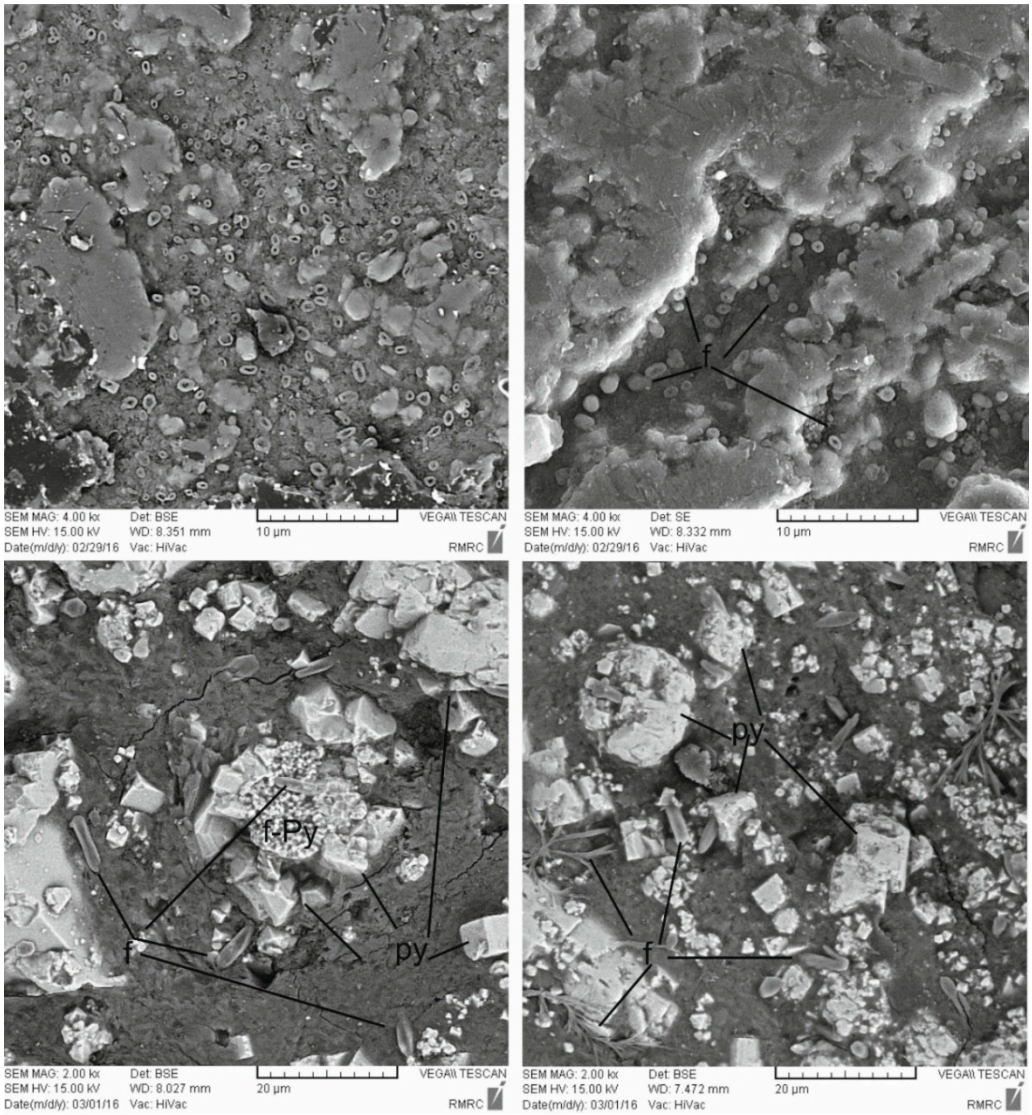

Figure 7. Representative back-scattered images showing different types of bacterial fossils and filamentous microorganisms (f) between pyrite (py: cubic pyrite; f-py: framboidal pyrite) in the Dopolan bauxite deposit.

6.2. Deposition Mechanisms of High-Grade Al Bauxite

It is well known that the solubilization of Al and Si in bauxite profiles is particularly sensitive to pH, but the rate of Fe mobility is mainly controlled by both pH and Eh [35–37]. In bauxite profiles, many factors can influence pH, such as organic matter content, CO_2 availability, standing electrolyte content, and the nature of the host rock [38,39]. The pH range in karstic bauxite is 5–9; however, most deposits have a pH range of 6–8. In the pH range of 5–9, the solubility of Si is 10–20 times greater than that of Al and Fe. Thus, after long-term weathering, significant dissolution of Si will have taken place, but Fe and Al will remain. For a constant environmental pH, the solubility of Fe can increase in competition to Al as a result of decreasing Eh [35,40,41]. Laskou and Economou-Eliopoulos [3] argued for a close relationship between iron leaching and alumina enrichment in the gray and red ores of the Parnassos–Ghiona deposits, Greece. The Dopolan bauxite deposit, with an average of 3% Fe, is essentially iron-poor bauxite (except for the pyrite-rich horizon, which has an average of 13% Fe). Fe leaching could take place during (syngenetic) or after (epigenetic) bauxite deposition [3,35]. Diaspore formed in a mildly reduced and alkaline environment and pyrite should precipitate under mildly acidic conditions. Therefore, the environmental conditions of the Dopolan bauxite deposit, based on the predominant ore minerals such as diaspore, pyrite, and kaolinite were changed from acidic reducing to slightly alkaline reducing (Figure 8). The existence of reducing conditions can also be deduced by the presence of the high content of organic matter. Field evidence such as the presence of plant root casts show that the Dopolan bauxite deposit formed in a swamp sedimentary basin. The high organic matter content of the Dopolan bauxite probably results from plant root casts as bauxite deposition was a preferred system for plant growth [18,42].

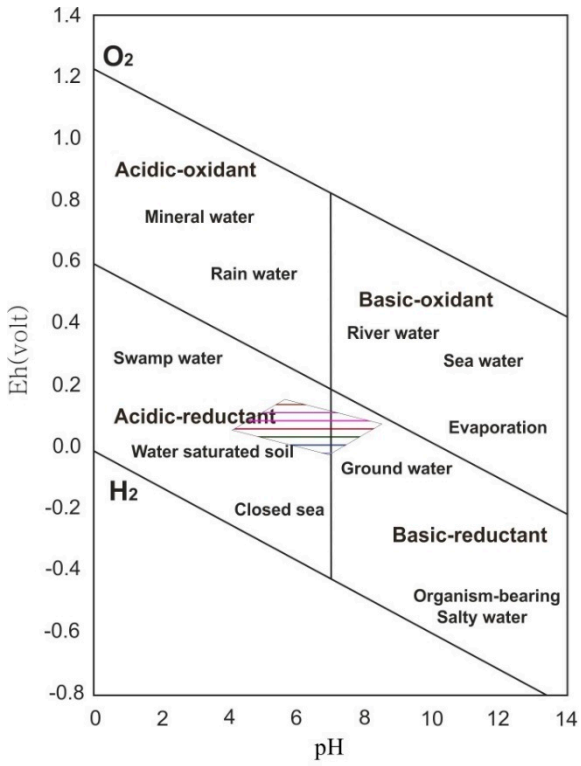

Figure 8. Eh–pH diagram illustrating the natural environmental conditions [40,43] of the stability fields of minerals in the Dopolan deposits. The thermodynamic data of the diagram were T = 25° and p = 1 bar.

Therefore, the main difference between the depositional environments of the Dopolan bauxite deposit and other Zagros bauxite deposits may be the greater reducing conditions, which caused Fe- leaching and Al enrichment (Table 4).

Table 4. Mineral descriptions and comparative Fe_2O_3, SiO_2, and Al_2O_3 contents of the Zagros bauxite deposits.

Deposit	Main Minerals	Al_2O_3 (wt %)	SiO_2 (wt %)	Fe_2O_3 (wt %)	Reference
Dopolan	diaspore–kaolinite–pyrite–nacrite	38–71	5–35	2–17	[18]
Sarfaryab	böhmite > gibbsite–calcite–kaolinite–hematite	18–63	6–14	2–18	[15]
Dehnow	böhmite–calcite–kaolinite–hematite	34–64	4–8	3–21	[16]
Mandan	böhmite–calcite–kaolinite–hematite	12–56	3–30	1–24	[16]
Hangam	böhmite–kaolinite–hematite–goethite	17–45	15–19	16–20	[14]

6.3. Mobility of REE and Trace Elements

The mobility of REE and trace elements in bauxite deposits is dependent on the physico-chemical conditions of pore water as it percolates through the soil [3,44–46]. Under oxidizing conditions, the solubility and deposition of REE are similar to those of Al_2O_3, P_2O_5, and TiO_2. In addition, the concentration of other immobile elements such as Zr, Nb, Ta, and Hf increase with increasing Al_2O_3, P_2O_5, and TiO_2 [47–49]. The REE can be absorbed by or adsorbed onto diaspore and böhmite. However, the high positive correlation between REE and P_2O_5 in the Dopolan karstic bauxite suggests that at the least some REE can be accommodated in the structure of some phosphates (i.e., Al-phosphates or members of the rhabdophane group). The mildly positive correlation of HFSE with TiO_2 suggests that these elements can be accommodated in the structure of TiO_2 polymorphs, as rutile. The highest contents of Al_2O_3, TiO_2, P_2O_5, Zr, Nb, Ta, and Hf were detected in the diaspore-rich bauxite, implying similarity of the geochemical characteristics during deposition (Figure 9) [50,51]. In contrast, the lowest contents of these elements were detected in the bauxitic kaolinite horizon with the lowest weathering rate and highest organic matter content. Therefore, the concentrations of these elements are mainly controlled by weathering factors [18,46,48,50–52]. The presence of organic matter in the bauxite profile caused reducing conditions, favoring the removal of REE and other immobile elements [3].

In contrast to REE and other immobile elements, which are enriched in the diaspore-rich horizon, the more mobile trace elements (e.g., Cu, Ni, Co, Cr, Pb, Zn, Sb, Ag, As, U, and V) are enriched in the pyrite-rich bauxite horizon with higher organic matter (0.37%) and lower Al_2O_3. These elements are more than twice as abundant in the pyrite-rich bauxite horizon (2200 ppm) than in the diaspore-rich (870 ppm) and clay bauxite (850 ppm) horizons. These elements appear to have been leached from the upper parts of the bauxitic profile and become precipitated in the lower part of the weathering profile in which the upper parts are more acidic and oxidizing but the lower pyrite-rich horizon is slightly acidic to alkaline and more reducing.

For the pH range 4–8 [53], it has been demonstrated that the mobility of most elements increased in soils with increasing Eh and vice versa. Additionally, some bacteria can play an important role in the mobility and precipitation of multiple redox state elements (e.g., Cu, Fe, Mn, Cr, and V) by means of their metabolic products [11,54–56]. Microorganism activity in the Dopolan bauxite deposit was demonstrated by microbial pyrite deposition (Section 6.2), and sulfur isotopic evidence (Section 6.4). Other important factors for the fixation of more mobile elements in the Dopolan deposit can be absorption by and/or adsorption onto the surface of pyrite and co-precipitation by clay minerals. Negatively charged surfaces of clay minerals offer extensive surfaces to adsorb positive charge elements largely in the pH range of 5 to 8 [7,10,11,54–56].

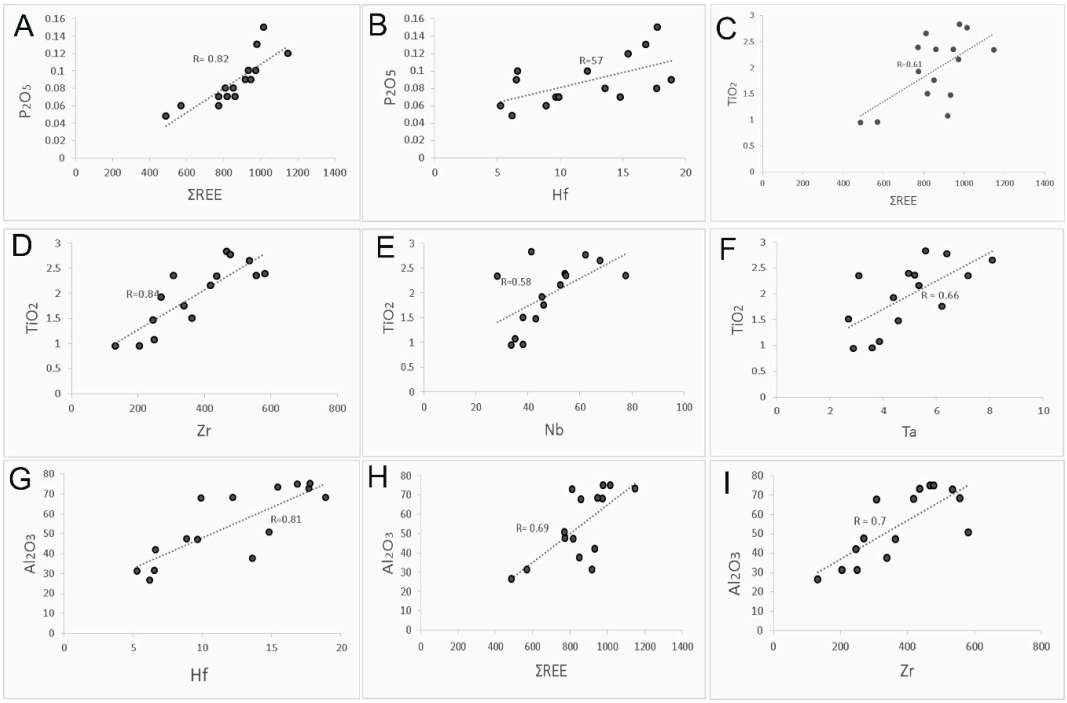

Figure 9. Variation diagrams showing the correlations between selected trace elements and Al_2O_3, P_2O_5, and TiO_2. Positive correlation between P_2O_5 and ∑REE (**A**); mildly positive correlation between P_2O_5 and Hf (**B**); mildly positive correlation between TiO_2 and ∑REE (**C**); Zr (**D**); Nb (**E**); Ta (**F**); Positive correlation between Al_2O_3 and Hf (**G**); mildly positive correlation between Al_2O_3 ∑REE (**H**); Zr (**I**).

6.4. Sulfur Isotope Constraints

The $\delta^{34}S$ values have been used as a tracer for biogenic sulfate reduction and reconstruction of paleoenvironments [57]. Pyrite formation in sedimentary and low-temperature environments has been well studied because of the relation between redox conditions and the biogeochemical cycles of sulfur, iron, and carbon [58]. The whole-rock and pyrite $\delta^{34}S$ values of the Dopolan bauxite deposit fall in a wide negative range, from −10‰ to −34‰, suggesting involvement of bacterial sulfate reduction after bauxitization. Sulfur isotope variation is dependent on the occurrence of sulfate reduction in an open or closed system [59]. Negative $\delta^{34}S$ values of pyrite imply fractionation by microorganisms during their sulfur metabolism by sulfate reduction in an open system [29,30,33]. The bacteria and microorganisms grew in a temperature range of 28–60 °C [60]. The negative sulfur values previously reported for Turkish bauxite deposits (Dogøankuzu and Mortas deposits; [1]) and the Parnassos–Ghiona deposit in Greece [4] are comparable to those of the Dopolan deposit and have been attributed to the reduction of sulfate by bacteria [4]. Surface water is the probable source of the sulfur, as indicated in other places [60,61].

7. Conclusions

The high-grade, gray-colored Dopolan bauxite deposit is found in the Triassic carbonates of the Khaneh Kat Formation. This deposit is a diaspore-rich karst-type bauxite with low Fe content and an unusual pyrite-rich horizon in the lowest part of the sequence. This study has focused on the role of organic matter and microorganisms in the bioleaching of elements, e.g., upgrading the alumina content of the deposit. The study offers the following conclusions:

1. The main minerals, such as diaspore, pyrite, kaolinite, and its association with preserved organic matter, suggest that bauxitization occurred in acidic reducing to slightly alkaline reducing conditions.

2. The low Fe content of the Dopolan bauxite implies that Fe leaching under reducing conditions may have resulted from organic matter in the presence of microbial activity. Fe was leached from the upper part of the bauxite profile and was deposited as pyrite in the lower part, generating a pyrite-rich bauxite horizon.
3. During the formation of the bauxite profile, less mobile elements, such as REE, Nb, Ta, Zr, and Hf, accumulated in the diaspore-rich horizon with higher alumina content, whereas redox sensitive elements such as Cr, Ni, Ag, Cu, Pb, Zn, U, and V, were concentrated in the pyrite-rich horizon.
4. Sulfur isotope data reveal a wide range of negative values of $\delta^{34}S$ for pyrite samples (from $-10‰$ to $-34‰$), suggesting the biogeochemical reduction of sulfate to sulfur.
5. Mineralogical data, geochemical evidence, and sulfur isotope data in this study suggest that biological activity played an important role in Fe remobilization, Al-upgrading, and the formation of the pyrite-rich horizon in the Dopolan bauxite deposit.

Acknowledgments: All financial support for this research was provided by the Research Office at Shiraz University, Iran. Iranian Mines & Mining Industries Development & Renovation (IMIDRO) is greatly acknowledged for support of the ICP-MS and XRD analyses. The CEO of the Dopolan bauxite mine is thanked for providing unlimited access to the Dopolan deposits. The Enago group is thanked for their assistance in editing the English. We would like to give our sincere thanks to Maria Economou-Eliopoulos of the University of Athens for reviewing an earlier version of the manuscript and constructive comments. Special thanks are extended to two anonymous reviewers for their valuable and constructive comments on the manuscript.

Author Contributions: Salamab Ellahi, Taghipour, and Nejadhadad conceived and designed the experiments; Taghipour, contributed reagents/materials/analysis tools; Nejadhadad, Taghipour and Salamab Ellahi wrote the paper.

Conflicts of Interest: The authors declare no conflict of interest.

References

1. Ozturk, H.; Hein, R.J.; Hanilci, N. Genesis of the Doğankuzu and Mortas, bauxite deposits, Taurides, Turkey: Separation of Al, Fe, and Mn and implications for passive margin metallogeny. *Econ. Geol.* **2002**, *97*, 1063–1077. [CrossRef]
2. Laskou, M.; Economou-Eliopoulos, M. Micro-organisms as fossils and present day development in Ni-laterites and bauxites of the Balkan Peninsula. In *Mineral Deposits Research Meeting the Global Challenge, Proceedings of the Eighth Biennial SGA Meeting, Beijing, China, 18–21 August 2005*; Mao, J., Bierlein, F.P., Eds.; Springer: Berlin/Heidelberg, Germany, 2005; pp. 1003–1006.
3. Laskou, M.; Economou-Eliopoulos, M. The role of microorganisms on the mineralogical and geochemical characteristics of the Parnassos-Ghiona bauxite deposits, Greece. *J. Geochem. Explor.* **2007**, *93*, 67–77. [CrossRef]
4. Laskou, M.; Economou-Eliopoulos, M. Bio-mineralization and potential biogeochemical processes in bauxite deposits: genetic and ore quality significance. *Mineral. Petrol.* **2012**, *73*, 124–140. [CrossRef]
5. Kalaitzidis, S.; Siavalas, G.; Skarpelis, N.; Carla Viviane Araujo, C.; Christanis, C. Late Cretaceous coal overlying karstic bauxite deposits in the Parnassus-Ghiona Unit, Central Greece: coal characteristics and depositional environment. *Int. J. Coal Geol.* **2010**, *81*, 211–226. [CrossRef]
6. Kalatha, S.; Economou-Eliopoulos, M. Framboidal pyrite and bacterio-morphic goethite at transitional zones between-Fe-Ni-laterite and limestones: Evidence from Lokris, Greece. *Ore Geol. Rev.* **2015**, *65*, 413–425. [CrossRef]
7. Lovely, D.R. Microbial reduction of iron, manganese, and other metals. *Adv. Agron.* **1995**, *54*, 175–231.
8. Berthelin, J. Microbial weathering processes. In *Microbial Geochemistry*; Krumbein, W.E., Ed.; Blackwell Scientific Publications: Oxford, UK, 1983; pp. 223–263.
9. Furrer, G.; Stumn, W. A coordination chemical approach to the kinetics of weathering. I. Dissolution of δ-Al_2O_3 and BeO. *Geochim. Cosmochim. Acta* **1986**, *50*, 1847–1860. [CrossRef]
10. McBride, M.; Sauvé, S.; Hendershot, W. Solubility control of Cu, Zn, Cd and Pb in contaminated soils. *Eur. J. Soil Sci.* **1997**, *48*, 337–346. [CrossRef]
11. Müller, B.; Axelesson, M.D.; Öhlander, B. Adsorption of trace elements on pyrite surfaces in sulfidic mine tailing from Kristenberg (Sweden) a few years after remediation. *Sci. Total Environ.* **2002**, *298*, 1–16. [CrossRef]

12. Lazo, O.; Cullaj, A.; Deda, T. Arsenic in soil environments in Albania. In *Arsenic in Soil and Groundwater: Biogeochemical Interactions*; Bhattacharya, P., Mukherjee, A.B., Zevenhoven, R., Loeppert, R., Eds.; Elsevier Book Series; Elsevier: Amsterdam, The Netherlands, 2007.
13. Oliveira, F.S.; Varajao, A.F.D.; Varajao, C.A.C.; Schaefer, C.E.G.R.; Bolange, B. The role of biogical agents in the microstructural and mineralogical transformations in aluminium lateritic deposit in Central Brazil. *Geoderma* **2014**, *226–227*, 250–269. [CrossRef]
14. Liaghat, S.; Hossini, M.; Zarasvandi, A. Determination of the origin and mass change geochemistry during bauxitization process at the Hangam Deposit, SE Iran. *Geochem. J.* **2003**, *37*, 627–637. [CrossRef]
15. Zarasvandi, A.; Charchi, A.; Carranza, E.J.M.; Alizadeh, B. Karst bauxite deposits in the Zagros mountain belt, Iran. *Ore Geol. Rev.* **2008**, *34*, 521–532. [CrossRef]
16. Zarasvandi, A.; Carranza, E.J.M.; Ellahi, S.S. Geological, geochemical, and mineralogical characteristics of the Mandan and Deh-now bauxite deposits, Zagros Fold Belt, Iran. *Ore Geol. Rev.* **2012**, *48*, 125–138. [CrossRef]
17. Calagari, A.A.; Abedini, A. Geochemical investigations on Permo-Triassic bauxite horizon at Kanisheeteh, east of Bukan, West-Azarbaidjan, Iran. *J. Geochem. Geoexplor.* **2007**, *93*, 232–576. [CrossRef]
18. Salamab Ellahi, S.; Taghipour, B.; Zarasvandi, A.; Bird, M.I.; Somarin, A.K. Mineralogy, Geochemistry and Stable Isotope Studies of the Dopolan Bauxite Deposit, Zagros Mountain, Iran. *Minerals* **2016**, *6*, 11.
19. Ehsanbakhsh, M.H.; Rahimzadeh, F. *Ardal Map 1; 100000*; Geological Survey and Mineral Exploration: Tehran, Iran, 1996.
20. Takin, M. Iranian geology and continental drift in the Middle East. *Nature* **1972**, *235*, 147–150. [CrossRef]
21. Agard, P.; Omrani, J.; Jolivet, L.; Mouthereau, F. Convergence history across Zagros, Iran: Constraints from collisional and earlier deformation. *Int. J. Earth Sci.* **2005**, *94*, 401–419. [CrossRef]
22. Walkey, A.; Black, I.A. An examination of Degtjareff method for determining soil organic matter, and proposed modification of the chromic acid titration method. *Soil Sci.* **1934**, *37*, 29–38. [CrossRef]
23. Baskar, S.; Baskar, R.; Kaushik, A. Role of microorganisms in weathering of the Konkan-Goa laterite formation. *Curr. Sci.* **2003**, *85*, 1129–1134.
24. Spatio, G. *The Geochemistry of Soil*; Oxford University Press: New York, NY, USA, 1989; p. 27.
25. Chapelle, F.H. *Ground-Water Microbiology and Geochemistry*; John Wiley & Sons: New York, NY, USA, 1993.
26. Berner, R.A. Biogeochemical cycles of carbon and sulfur and their effect on atmospheric oxygen over Phanerozoic time. *Palaeogeogr. Palaeoclimatol. Palaeoecol.* **1989**, *75*, 97–122. [CrossRef]
27. Jensen, M.L. Sulfur isotopes and mineral genesis. In *Geochemistry of Hydrothermal Ore Deposits*; Barnes, H.L., Ed.; Holt, Rinehart, and Winston: New York, NY, USA, 1967; pp. 143–165.
28. Ohmoto, H.; Rye, R.O. Isotopes of sulfur and carbon. In *Geochemistry of Hydrothermal Ore Deposits*; Barnes, H.L., Ed.; Wiley and Sons: New York, NY, USA, 1979; pp. 509–567.
29. Ohmoto, H.; Goldhaber, M.B. Sulfur and carbon isotopes. In *Geochemistry of Hydrothermal Ore Deposits*; Barnes, H.L., Ed.; Wiley and Sons: New York, NY, USA, 1997; pp. 517–611.
30. Seal, R. *Sulfur Isotope Geochemistry of Sulfide Minerals*; U.S. Geological Survey Staff-Published Research: Reston, VA, USA, 2006; p. 345.
31. Roedder, E. The noncolloidal origin of "colloform" textures in sphalerite ores. *Econ. Geol.* **1968**, *63*, 451–471. [CrossRef]
32. Anderson, G.M. The mixing hypothesis and the origin of Mississippi Valley-type ore deposits. *GeoFluids* **2008**, *103*, 1683–1690. [CrossRef]
33. Nejadhadad, M.; Taghipour, B.; Zarasvandi, A.K.; Somarin, A. Geological, geochemical, and fluid inclusion evidences for the origin of the Ravanj Pb–Ba–Ag deposit, north of Delijan city, Markazi Province, Iran. *Turk. J. Earth Sci.* **2016**, *25*, 179–200. [CrossRef]
34. Wang, H.; Morse, H.C. IRF8 regulates myeloid and B lymphoid lineage diversification. *Immunol. Res.* **2009**, *43*, 109–117. [CrossRef] [PubMed]
35. Patterson, S.H. *Bauxite Reserves and Potential Aluminum Resources of the World*; U.S. Geological Survey: Reston, VA, USA, 1967; pp. 1228–1258.
36. Brimhall, G.H.; Lewis, C.J.; Ague, J.J.; Dietrich, W.E.; Hampel, J.; Teague, T.; Rix, P. Metal enrichment in bauxites by deposition of chemically-mature aeolian dust. *Nature* **1988**, *333*, 819–824. [CrossRef]
37. Ehrlich, H.L.; Wickert, L.M.; Noteboom, D.; Doucet, J. *Weathering Pisolitic Bauxite by Heterotrophic Bacteria*; University of Chile: Santiago, Chile, 1995; Volume I, pp. 395–403.
38. McLean, E.D. Chemistry of soil aluminum. *Commun. Soil Sci. Plant Anal.* **1976**, *7*, 619–636. [CrossRef]

39. Thomas, G.W. Soil pH and Soil Acidity. In *Methods of Soil Analysis: Chemical Methods*; Soil Sciences Society of America/American Society of Agronomy: Madison, WI, USA, 1996; Part 3; pp. 475–496.
40. Liu, X.; Wang, Q.; Feng, Y.; Cai, Z. Genesis of the Guangou karstic bauxite deposit in western Henan, China. *Ore Geol. Rev.* **2013**, *55*, 162–175. [CrossRef]
41. Zhang, Z.; Zhou, L.; Li, Y.; Wu, C.; Zheng, C. The "coal–bauxite iron" structure in the ore-bearing rock series as a prospecting indicator for southeastern Guizhou bauxite mines. *Ore Geol. Rev.* **2013**, *53*, 145–158. [CrossRef]
42. Buchanan, S.J.; So, H.B.; Kopittk, P.M.; Menzies, N.W. Influence of texture in bauxite residues on void ratio, water holding characteristics, and penetration resistance. *Geoderma* **2010**, *158*, 421–426. [CrossRef]
43. Garrels, R.; Christ, L.C. *Solutions, Minerals, and Equilibria*; John Wiley: New York, NY, USA, 1965; 450p.
44. Maksimovic, Z.; Panto, G. Contribution to the geochemistry, of rare earth elements in the karst-bauxite deposits of Yugoslavia and Greece. *Geoderma* **1991**, *51*, 93–109. [CrossRef]
45. Carrillo-González, R.; González-Chávez, M. Metal accumulation in wild plants surrounding mining wastings. *Environ. Pollut.* **2006**, *144*, 84–92. [CrossRef] [PubMed]
46. Meshram, R.R.; Randiv, K.R. Geochemical study of laterites of the Jamnagar district, Gujarat, India: implications on parent rock, mineralogy and tectonics. *J. Asian Earth Sci.* **2011**, *42*, 1271–1287. [CrossRef]
47. Mordberg, L.E.; Spratt, J. Alteration of zircons: The evidence of Zr mobility during bauxitic weathering. In Proceedings of the Goldschmidt Conference Toulouse, Toulouse, France, 30 August–3 September 1998; pp. 1021–1022.
48. Hill, I.G.; Worden, R.H.; Meighan, I.G. Geochemical evolution of a palaeolaterite: The Interbasaltic Formation, Northern Ireland. *Chem. Geol.* **2000**, *166*, 65–84. [CrossRef]
49. Karadag, M.M.; Kupeli, S.; Aryk, F.; Ayhan, A.; Zedef, V.; Doyen, A. Rare earth element (REE) geochemistry and genetic implications of the Mortas bauxite deposit (Seydisehir/Konya-Southern Turkey). *Chemie der Erde* **2009**, *69*, 143–159. [CrossRef]
50. Laufer, F.; Yariv, S.; Steinberg, M. The adsorption of quadrivalent cerium by kaolinite. *Clay Miner.* **1984**, *19*, 137–149. [CrossRef]
51. Mongelli, G. Ce-anomalies in the textural components of Upper Cretaceous karst bauxites from the Apulian carbonate platform (southern Italy). *Chem. Geol.* **1997**, *14*, 69–79. [CrossRef]
52. Roaldest, E. Mineralogical and Chemical Changes during Weathering, Transportation and Sedimentation in Different Environments. Ph.D. Thesis, University of Oslo, Oslo, Norway, 1978.
53. Forstner, U. Metal speciation–general concepts and applications. *Int. J. Environ. Anal. Geochem.* **1993**, *51*, 5–23. [CrossRef]
54. Kersten, M.; Forstner, U. Geochemical characterization of the potential trace metal mobility in cohesive sediments. *Geo-Mar. Lett.* **1991**, *11*, 184–187. [CrossRef]
55. Nealson, K.H.; Stahl, D.A. Microorganisms and biogeochemical cycles: What can we learn from layered microbial communities. *Rev. Mineral.* **1997**, *35*, 5–34.
56. Ehrlich, H.J. *Geomicrobiology*, 4th ed.; Marcel Dekker: New York, NY, USA, 2002; p. 800.
57. Strauss, H.; Scchieber, J. A sulfur isotope study of pyrite genesis: The Mid-Protezoic Newland Formation, Belt supergroupe, Montana. *Geochim. Cosmochim. Acta* **1990**, *54*, 197–204. [CrossRef]
58. Goldhaber, M.B. *Sulfur-Rich Sediments. Treatise on Geochemistry: Sediments, Diagenesis, and Sedimentary Rocks*; Elsevier: Amsterdam, The Netherlands, 2003; Volume 7, pp. 257–288.
59. Hoefs, J. *Stable Isotope Geochemistry*, 6th ed.; Springer: Berlin, Germany, 2009; p. 285.
60. Smock, A.M.; Bottcher, M.E.; Cypionka, H. Fractionation of sulfur isotopes during thiosulfate reduction by Desulfovibrio desulfuricans. *Arch. Microbiol.* **1998**, *169*, 460–463. [CrossRef] [PubMed]
61. Smith, D.W.; Rittenberg, S.C. On the sulfur-source requirement for growth of Thiobacillus intermedius. *Arch. Microbiol.* **1974**, *100*, 65–71. [CrossRef] [PubMed]